Computer Networks 179 (2020) 107370

Contents lists available at ScienceDirect

Computer Networks

journal homepage: www.elsevier.com/locate/comnet

The TeraNova platform: An integrated testbed for ultra-broadband wireless communications at true Terahertz frequencies

Priyangshu Sen[a], Dimitris A. Pados[b], Stella N. Batalama[b], Erik Einarsson[c,d], Jonathan P. Bird[c], Josep M. Jornet[a,*]

[a] Department of Electrical and Computer Engineering, Northeastern University, United states
[b] College of Engineering and Computer Science at Florida Atlantic University, United states
[c] Department of Electrical Engineering, University at Buffalo, United states
[d] Department of Materials Design and Innovation, University at Buffalo, United states

ARTICLE INFO

Keywords:
Terahertz communications
Ultra-broadband networking
Testbed and experimental research
6G

ABSTRACT

Terahertz (THz)-band (0.1 THz to 10 THz) communication is envisioned as a key technology to meet the demand for faster, more ubiquitous wireless communication networks. For many years, the lack of compact, fast and efficient ways to generate, modulate, detect and demodulate THz-band signals has limited the feasibility of such communication systems. Recently, major progress within different device technologies is finally closing the so-called THz gap. For the time being, communication testbeds have been developed at sub-THz frequencies, i.e., at or near the boundary with millimeter-wave communication systems. Nonetheless, higher carrier frequencies and their associated bandwidth are needed to meet the demand for much higher data rates. In this paper, the TeraNova platform, i.e., the first integrated testbed for ultra-broadband wireless communications at *true* THz-band frequencies, is presented. The system consists of a transmitter and a receiver based on Schottky-diode frequency multiplying and mixing chains able to up & down-convert an information-bearing intermediate frequency (IF) signal up to 40 GHz-wide between 1 and 1.05 THz, i.e., the first absorption-defined transmission window above 1 THz. Guided by the experimental characterization of the THz channel in terms of path-loss and noise, tailored framing, time synchronization, channel estimation and single- and multi-carrier modulation techniques are implemented in software and realized by a state-of-the-art arbitrary waveform generator and a digital storage oscilloscope at the transmitter and the receiver, respectively. Experimental results are presented herein to highlight the opportunities and challenges to unleash the potential of the THz band.

1. Introduction

Wireless data traffic has surged in recent years due to a change in the way today's society creates, shares, and consumes information. Accompanying this change is an increasing demand for faster, more ubiquitous wireless communication networks. As a result, wireless Terabit-per-second (Tbps) links are expected to become a necessity within the next five to ten years. Several alternatives are being considered to meet this demand. On the one hand, the development of sophisticated physical layer techniques (e.g., massive MIMO communications & AI-infused signal processing) and the adoption of frequency sub-bands in the millimeter-wave spectrum (e.g., 28 GHz & 60 GHz bands) are part of 5G systems able to support data rates approaching 100 Gigabits-per-second (Gbps). On the other hand, optical wireless communication (OWC) systems, whether at infra-red, visible or even ultra-violet frequencies, are also being explored for future ultra-broadband wireless communication systems able to support physical-layer data-rates exceeding 100 Gbps.

Between these regions of the electromagnetic (EM) spectrum, the Terahertz (THz) band (from 100 GHz to 10 THz) has recently attracted the attention of the wireless communication community [1,2]. This band provides huge transmission bandwidths (much larger than at mm-wave frequencies), which range from a few THz for distances below one meter to multiple transmission windows each tens to hundreds of GHz wide for longer distances. Nevertheless, this very large bandwidth comes at the cost of a high propagation loss (yet still lower than at optical frequencies), resulting from spreading and molecular absorption, which also creates a unique distance dependence on the available bandwidth. All these require the development of innovative solutions. For the time being, the majority of THz-band communication works are mainly theoret-

* Corresponding author.
E-mail address: jmjornet@northeastern.edu (J.M. Jornet).

https://doi.org/10.1016/j.comnet.2020.107370
Received 25 March 2020; Received in revised form 5 June 2020; Accepted 14 June 2020
Available online 15 June 2020

ical or contain limited experimental validation (always in the sub-THz range or under 1 THz), because of the absence of experimental platforms for *true* THz communications.

The lack of compact high-power signal sources, high-speed modulators & demodulators, and high-sensitivity detectors able to work at room temperature has traditionally hampered the use of the THz band for any application beyond sensing. However, many recent advancements with several different device technologies are closing the so-called THz gap [3]. In an *electronic approach*, the limits of standard silicon CMOS technology [4], silicon-germanium BiCMOS technology [5] and III–V semiconductor transistor [6] and Schottky diode [7] technologies are being pushed to reach the 1 THz mark. In a *photonics approach*, uni-traveling carrier photodiodes [8], photoconductive antennas [9], optical downconversion systems [10] and quantum cascade lasers [11] are being investigated for THz systems. More recently, the use of nanomaterials such as graphene is enabling the development of plasmonic devices [12]. These devices are intrinsically small, operate efficiently at THz frequencies, and can support large modulation bandwidths. Moreover, graphene is just the first of a new generation of 2D materials, which can be stacked to create new types of devices that leverage new physics.

Experimental testbeds for THz communications can be developed using the technologies mentioned above. These platforms should integrate at least one transmitter and one receiver, and should ideally be able to support multi-GHz bandwidths over THz-band carrier frequencies. Existing platforms (Section 2) still operate at carrier frequencies below 1 THz with baseband bandwidths of up to a few tens of GHz. It is expected that, in order to enable wireless Tbps, a larger channel bandwidth and devices fast enough to utilize it are needed. These two conditions can be met by exploring higher-frequency windows, specifically around 1 THz and above.

In this paper, we introduce the TeraNova platform, the first integrated testbed for ultra-broadband wireless communications at true THz-band frequencies. In a nutshell, the TeraNova hardware (Section 3) consists of: a state-of-the-art arbitrary waveform generator (AWG) able to generate baseband signals with an analog bandwidth up to 32 GHz per channel; a Schottky-diode-based THz signal source and mixer capable of up-converting a tunable 40.8 GHz to 43.75 GHz local oscillator (LO) signal anywhere between 0.98 and 1.05 THz; directional THz antennas; a Schottky-diode-based broadband THz receiver capable of down-converting the received signals; and a state-of-the-art high-performance digital storage oscilloscope (DSO), with 63 GHz analog bandwidth.

Guided by the first experimental characterization of the 1 THz channel reported in this work, in terms of both path-loss as well as amplitude and phase noise, we design and implement a tailored physical layer in software at the AWG and DSO. This incorporates framing, time synchronization, channel estimation and single and multi-carrier modulation and demodulation functionalities (Section 4) and, given the nature of the AWG/DSO, entails offline signal processing. Experimental results are provided (Section 5) to illustrate the behavior of the wireless channel at 1 THz and the performance of different modulation schemes. Finally, we discuss (Section 6) the challenges that need to be overcome in order to unleash the potential of the THz band, particularly on how to increase the communication distance and data-rates and expand the range of applications from on-chip, short-range device-to-device communications and wireless personal network areas, to local area networks, small networks, wireless backhaul and beyond.

2. Existing Terahertz communications testbeds

Several groundbreaking experimental testbeds for THz-band communications have been developed within the last decade. Here we focus on THz platforms (not mm-wave or OWC) that support the transmission of actual data, and exclude systems aimed at sensing applications or channel characterization only. In the seminal work in [13], a sub-harmonic mixer based on Schottky diodes was utilized to up-convert a 10 GHz baseband signal to 300 GHz by using a chain of frequency multipliers. An analog video was transmitted over a distance of 20 m, down-converted by a similar setup and decoded by an analog TV card. An improved platform was utilized in [14] to transmit standard high-definition digital video over a distance of 50 m. In these two experiments, standard analog/digital video signals were generated, transmitted, received and processed. In [15], an experimental testbed able to operate at 625 GHz was reported. A chain of frequency multipliers based on Schottky diodes was utilized to directly up-convert the modulated baseband signal. A zero-bias Schottky diode operating in direct detection mode was used as a broadband receiver. Data transmission at 2.5Gbps was achieved when utilizing non-return-to-zero on-off keying modulation.

In [16], an InP-based frequency doubler, mixer, and amplifier were utilized to create a wireless link at 220 GHz. Data rates up to 10 Gbps at 2 m and 25 Gbps at 0.5 m were shown. In [17], the same authors utilized a revised platform based on the same technology to transmit over a distance of 10 m with data rate up to 25 Gbps at 220 GHz. In [18], a photodiode emitter and a Schottky diode detector were used to experimentally create a link at 300 GHz able to support 24 Gbps. In [19], a system composed of a high-power photonic transmitter and a MMIC-based receiver at 237.5 GHz with 35 GHz bandwidth was used to create a stable 100 Gbps rate over 20 m. More recently, the goal has been to increase the communication distance, generally by leveraging very-high-gain directional antennas (above 50 dB) at 240 GHz [20] and 667 GHz [21]. Other relevant works include [22], where a 4-channel MIMO at 300 GHz is demonstrated, or [23], where commercial silicon photonics technology is utilized to demonstrate a 56 Gbps link at 300 GHz.

A comparative summary of these works is provided in Table 1. In all the aforementioned systems, the carrier frequency is well below 1 THz. In addition, their focus is on demonstrating the hardware capabilities, while implementing none or only standardized solutions for the physical layer, including framing, synchronization, channel estimation and equalization, and modulation/demodulation.

In this paper, we report a state-of-the-art platform to guide the development of communication solutions tailored to the capabilities of THz devices and the peculiarities of the THz channel. Many have been the challenges that we had to overcome. With the commercially accessible technology, a maximum of -15 dBm (30 μW) of transmitter power is available, which restricts ultra-broadband communication to line of sight (LoS) propagation over up to 20-cm-long distances. Furthermore, highly directional antennas are utilized to acquire the required signal power. At the receiver, due to the unavailability of low noise amplifiers (LNAs) at THz frequencies, a low noise mixer is utilized as the first element after the receiver antenna to retain the noise figure (NF) in a considerable range. However, an ultra-broadband LNA is utilized at the IF stage to amplify the signal for proper acquisition of the waveform. In addition, a tailored software-based physical layer is designed to solve the issues affecting ultra-broadband signals including distortion due to the non-flat hardware frequency response and high noise power. A pre-equalizating filter is utilized at the transmitter to compensate for the hardware deterministic frequency-selective response, which reduces the noise power enhancement at the receiver side. To synchronize the starting point of the signal at a low SNR regime, an engineered maximum merit factor (MF) sequence is utilized. To restrict the noise power, we use a band-pass noise filter at the receiver. Also, we take advantage of oversampling gain, which is incorporated with the correlator-type detector. Moreover, to restrict the phase noise within the limit, the frame transmission duration is restricted. Besides, the low peak to average power ratio (PAPR) modulation schemes are suggested for THz band communications. The full details are provided in the next sections.

3. TeraNova hardware overview and specifications

The block diagram of the TeraNova testbed is illustrated in Fig. 1. On the transmitter side, a high-performance analog signal generator (PSG) is utilized to synthesize the LO. A Schottky-diode-based chain of

Table 1
Comparison of the existing experimental testbeds for THz communications.

Reference	Carrier frequency	Distance	BW/ Data rate	Channel estimation/ Equalization/ Synchronization	Frame structure	Data	Year
[13]	300 GHz	22 m	10 GHz / –	Analog filtering	Analog Video	Analog video signal	2008
[14]	300 GHz	50 m	8 MHz / –	DVB protocol	DVB	DVB signal	2010
[15]	625 GHz	Few meters	5 GHz / 2.5 Gbps	NA	NA	NRZ signal	2011
[16]	220 GHz	50 cm	50 GHz/25 Gbps	NA	NA	Bit pattern generator	2011
[16]	220 GHz	2 m	50 GHz / 10 Gbps	DVB protocol	DVB	DVB signal	2011
[17]	220 GHz	10 m	40 GHz / 25 Gbps	NA	NA	User-defined	2012
[18]	300 GHz	50 cm	35 GHz / 24 Gbps	NA	NA	User-defined	2012
[19]	237.5 GHz	20 m	35 GHz / 100 Gbps	NA	NA	User-defined	2013
[20]	240 GHz	850 m	40 GHz / 64 Gbps	NA	NA	User-defined	2015
[21]	666 GHz	590 m	– / 9.5 Gbps	NA	Header + Payload	User-defined	2017
[22]	300 GHz	50 cm	– / 56 Gbps	NA	NA	User-defined	2017
[23]	300 GHz	5 m	– / 16 Gbps	NA	NA	User-defined	2019
This work	1025 GHz	16 cm	30 GHz / 30 Gbps	ML estimation equalization 18-bit MF sequence	Header + Pilots + Payload	User-defined	2020

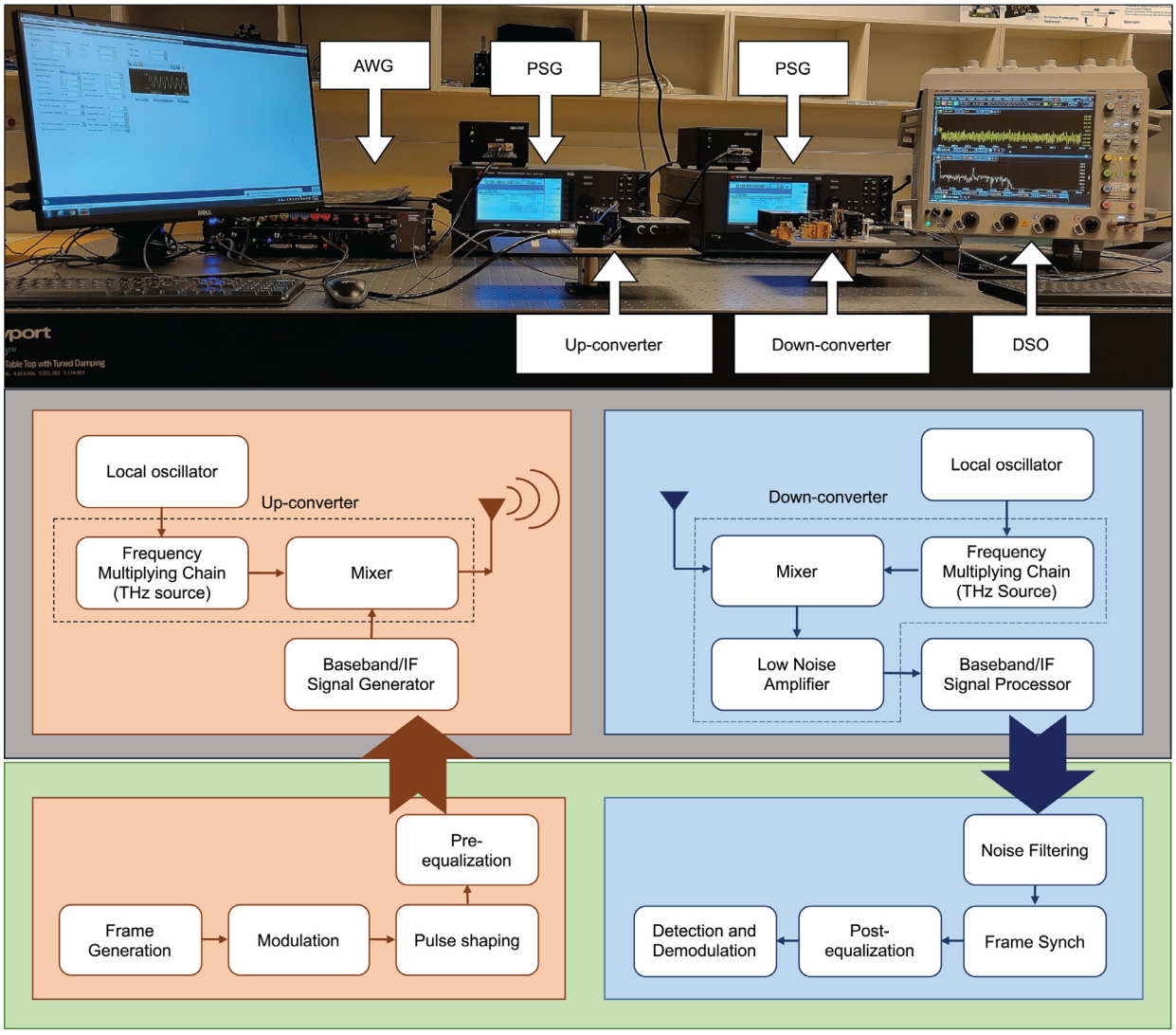

Fig. 1. The Teranova testbed (top); schematic diagram of the TeraNova hardware components (middle); and diagram of the physical layer design and implementation for transceiver system (bottom).

frequency multipliers is utilized to up-convert the LO to the target radio frequency (RF) between 0.98 THz and 1.05 THz. The RF frequency is mixed with the intermediate frequency (IF) signal by means of a broadband mixer based on the same technology. The IF signal is generated by means of a state-of-the-art AWG by utilizing the physical layer described in Section 4. On the receiver side, a second PSG and frequency multiplier chain and mixer are utilized to generate the LO frequency and RF carrier, needed to down-convert the received RF frequency to IF band. A state-of-the-art DSO is utilized to digitize and store the received signals for further processing. Processing of the digitized signals is done by the physical layer described in Section 4. Next, we describe the main system blocks at the transmitter and the receiver.

3.1. Transmitter

The first element at the transmitter side is an analog signal generator (Keysight E8257D), which can create very stable sinusoidal signals between 250 kHz and 50 GHz with low root mean square (RMS) jitter (21fs). In our case, the PSG is set between 40.8 GHz and 43.75 GHz.

To up-convert the LO to true THz frequencies, a frequency multiplier, mixer and amplifier chain (MixAMC), based on Schottky-diode technology and custom-designed by Virginia Diode Inc. (VDI), is used. The frequency chain consists of four multipliers (three frequency doublers and one frequency tripler, total multiplication factor $\times 24$) and is used to generate a carrier signal anywhere between 0.98 THz and 1.05 THz. This supports the testing of THz communication systems on the first absorption-defined transmission window above 1 THz, i.e., from 1.0 THz to 1.05 THz, which is the focus of our study, but also allows the characterization of the absorption line at 980 GHz. Following the MixAMC, a sub-harmonic frequency mixer is used to modulate the carrier signal with the information-bearing IF signal. The mixer is able to operate with broadband signals between 100 kHz and 40 GHz and exhibits a double sideband conversion loss of less than 15 dB. The maximum input power at IF is 0 dBm and the maximum output power is -15 dBm or 30 μW.

To generate an ultra-broadband (tens of GHz wide) information-carrying IF signal, a state-of-the-art AWG (Keysight M8196A) with high bandwidth baseband signal processing capabilities is utilized. The AWG incorporates four Digital-Analog-Converters (DACs), with an analog bandwidth in excess of 32 GHz, a sampling frequency of up to 93.4 Gigasamples-per-second (GSaps) and 8-bit point resolution. Besides conventional pre-defined waveforms, the AWG is utilized in our case to generate any user-defined signal with up to 512 kSa. The maximum output power of the device is 10 dBm for the single end output and 13 dBm for the differential output. Any mathematically-defined waveform represented by a series of discrete points can be generated with high precision.

3.2. Receiver

At the receiver side, an identical setup (LO + MixAMC) is utilized to generate a THz carrier signal, which in this case is mixed with the received RF signal to recover the IF signal. Here, the required LO signal is generated by analog signal generator (Keysight E8257D), which is identical but separate than transmitter section. Down-converter is Schottky-diode-based frequency multiplier, mixer and amplifier (MixAMC) from Virginia Diode Inc. Similar to up-converter it has four multipliers (3 frequency doublers and 1 frequency tripler) chain, which is responsible for the down-conversion 1 THz RF signal to the baseband signal. The down-converter has double sideband conversion loss of 15 dB and incorporates a low noise amplifier (LNA) with 10 dB gain. Due to the challenges in designing an LNA with low NF at higher frequencies and, consequently, the unavailability of an LNA in our frequency range of interest, an LNA is utilized only at the IF stage (DC-40 GHz) to amplify the received signal power. The intention is to use the full DSO by maintaining the received signal amplitude above the DSO sensitivity (i.e., >1 mv). Moreover, to maintain the NF in a tolerable range, a low noise mixer is utilized as the first element after the receiver antenna.

A DSO (Keysight DSOZ632A) is utilized for real-time signal acquisition, observation and storage. The DSO capable of capturing ultra-broadband signals with up to 63 GHz, enabled by an Analog-to-Digital Converter (ADC) with a sampling frequency of 160 GSaps, with 8-bit resolution, and capacity for up to 100 Mpts. The system has low RMS jitter of 170 fs and low RMS noise floor of 1 mV to 63 mV.

3.3. Other elements

Two directional diagonal horn antennas are used to radiate and detect the RF signal. Each antenna exhibits a gain of 26 dBi and 10° angle 3 dB bandwidth at the design frequency of 1 THz. The antenna and the mixer are connected by means of a rectangular waveguide (WR-1.0).

To interconnect the different testbed elements, 2.4 mm coaxial cables are used. The losses of these cables at the LO and IF frequencies are non-negligible, ranging from 2.5 dB/m at 6 GHz to 8 dB/m at 40 GHz. VSWR rating of the connectors is approximately 1.2:1, thus introduce another 0.36 dB of insertion loss. Given the low power and high channel losses, every loss directly impacts system performance. This fact motivates the need to develop integrated on-chip THz systems.

4. TeraNova physical layer design and implementation

In this section, we discuss the physical layer for the transmitter and the receiver (Fig. 1). At the transmitter, the user-provided data bits are structured in frames, modulated into symbols and shaped into digital signals to be fed to the AWG. At the receiver, the digitized signals captured by the DSO are synchronized, equalized and demodulated to recover the data bits. MATLAB is utilized at both ends, which drastically simplifies the design of the different signal processing blocks and ensures a rapid transition from numerical analysis to experimental testing. While we describe the reference design currently implemented in the platform, any of the blocks can be easily replaced to support the testing of new functionalities, making the TeraNova a true testbed for THz communications. We divide the physical layer components into transmitter and receiver side blocks to describe their detailed functionality.

4.1. Transmitter

Initially, the frame is generated by adjoining three parts, namely, header, training sequence and data sequence. The header (18 bits) is a maximal merit factor (MF) sequence, which we demonstrated [24] offers optimal correlation properties (high auto-correlation and low cross-correlation) and, thus, is uniquely suited to detect the beginning of a new frame in low signal to noise ratio (SNR) scenario. The training sequence (up to 200 bits) contains the bits that will be used for channel estimation and equalization purposes. The data sequence contains up to 2184 user-defined bits. As we will discuss in Section 5, this length is determined after taking the phase noise of the system into consideration.

The generated frames are modulated according to different single-carrier or multi-carrier modulation schemes. For single carrier modulations, M-ary Pulse Amplitude Modulation (M-PAM) and M-ary Phase Shift Keying (M-PSK) are considered. The in-phase (I_m) and quadrature (Q_m) components are calculated to generate each symbol x_m, where $m = 1, 2, \ldots, M$ and M is the modulation index. For M-PAM, the I_m and Q_m components are given by

$$I_m = 2m - 1 - M; Q_m = 0, \tag{1}$$

and, for M-PSK, these correspond to

$$I_m = \cos\left(\frac{(m-1)}{M}2\pi\right); Q_m = \sin\left(\frac{(m-1)}{M}2\pi\right). \tag{2}$$

For the testing of multi-carrier modulations, orthogonal frequency division multiplexing (OFDM) is implemented. In this case, the generated in-phase and quadrature components ($I_m + jQ_m$) for each carrier

are passed through a serial-to-parallel conversion block, then fed to an IFFT block. A cyclic prefix is added to increase the robustness against inter symbol interference (ISI). For transmission, the time domain symbols are passed through a parallel-to-serial converter. Equalization is done by sending known $I_m + jQ_m$ values in regular carrier intervals.

The modulated symbols are passed through a root raised cosine pulse filter, which helps to restrict the generated signals' spectrum within the transmission bandwidth and, at the receiver, eases the noise filtering process. Under the assumption of additive Gaussian noise at the receiver, the resulting signal x_m is given by

$$x_m(t) = Re\{p(t)(I_m + jQ_m)\exp(j2\pi f_{IF}t)\}, \tag{3}$$

where t refers to time, p is the raised cosine pulse and f_{IF} refers to the intermediate frequency.

Finally, pre-equalization, also often referred to as pre-distortion, is implemented to compensate for the hardware deterministic frequency-selective response. In our case, this arises mainly from the frequency-dependent attenuation of the coaxial cables and connectors. The measured frequency response of each component is estimated as,

$$H(k) = \left(\frac{P_r(k) - P_n}{P_s(k)}\right)^{1/2}, \tag{4}$$

where P_r is the received signal power with noise at the k_{th} frequency, P_s refers to the transmitted signal power and P_n is noise power for whole observation bandwidth. The inverse of H is then used to pre-distort the signals to be transmitted. As the pre-equalization is implemented in the transmitter side, it does not provide any noise enhancement at the receiver side.

4.2. Receiver

At the receiver side, a Parks-McClellan designed Chebyshev bandpass filter, and a low pass filter are utilized to eliminate the out of band noise for M-PSK and M-PAM, respectively. This improves the SNR by reducing the out of the band electromagnetic interference and noise at the different stages of the receiver.

The frame synchronization block is utilized to detect the starting point of the captured signal. This block correlates the received signal with the same 18-bit-long maximal MF sequence utilized at the transmitter.

A minimum mean square error (MMSE) linear filter equalizer is utilized to mitigate the effect of the frequency selective nature of the channel and path loss. The filter coefficient vector $\hat{f}$ for post-equalization is obtained by minimizing the error between the transmitted training symbols, $\hat{s}$, and the symbols of the output of the equalizer, i.e., $R\hat{f}$, where R is the Toeplitz matrix with the received training symbols. The channel model is given by

$$r(n) = h(n) * s(n) + v(n), \tag{5}$$

where s is the transmitted pilot signal to estimate the channel, r stands for the received signal, v are the noise samples and h is the channel coefficient. Therefore, the optimization function w.r.t. $\hat{f}$ is formulated as,

$$\min||\hat{s} - R\hat{f}||^2, \tag{6}$$

where $\hat{s}^T = [s(n+1)s(n+2)\dots s(p)]$ is the transmitted pilot signal vector till p_{th} instant, $\hat{f}^T = [f(0)f(1)\dots f(n)]$ stands for the $n+1$ tap equalizer coefficient vector, and $R((p-n)\times(n+1))$ is given by,

$$\boldsymbol{R} = \begin{bmatrix} r(n+1) & r(n) & r(n-1) & \dots & r(1) \\ r(n+2) & r(n+1) & r(n) & \dots & r(2) \\ \vdots & \vdots & \vdots & \ddots & \vdots \\ r(p) & r(p-1) & r(p-2) & \dots & r(p-n) \end{bmatrix}, \tag{7}$$

By solving the minimization Eq. (6), we obtain the post-equalizer filter coefficient as,

$$\hat{f} = (R^T R)^{-1} R^T \hat{s}. \tag{8}$$

The equalized signal waveform is passed through a correlator-type detector and the maximum likelihood (ML) criterion is utilized to recover the bits. In this case, every possible symbol is correlated with the received symbol and the maximum match gives the decision for the detection of bits. This is an optimal detector provided that the receiver experiences additive Gaussian noise, which is discussed Section 5.3. The ML correlator detection process is illustrated as,

$$\hat{m} = \arg\max_{1\le m\le M}\left(\int_0^T r(t).x_m(t)\,dt - \frac{1}{2}||x_m||^2\right) \tag{9}$$

where, $\hat{m}$ is the maximum match with a particular symbol and used for bit detection. Furthermore, $m = 1, 2, \dots, M$, and M denotes the modulation index. $r(t)$ refers to the received symbol. Besides, the oversampling gain [25,26] incorporated in the maximum likelihood (ML) correlator-type detector assists in improving the effective SNR.

In the case of OFDM, the cyclic prefix is removed from the received data and then passed through a serial to parallel conversion block. The output is fed to an FFT block to recover the corresponding complex baseband symbols in $I_m + jQ_m$ form. The complex baseband symbols are passed through the detection algorithm.

5. Experimental system characterization and tests results

5.1. Link budget analysis

We first theoretically calculate and experimentally validate the link budget for the system, by taking into account the loss introduced by every element. In particular, the received signal power P_{rx} in dB is given by,

$$P_{rx} = P_{tx} + G_{tx} + G_{rx} + G_{LNA} - L_{spread} - L_{abs} - L_{mixer} - L_{misc}, \tag{10}$$

where P_{tx} is the transmitted signal power, G_{tx} and G_{rx} are the transmit and receive antenna gains, respectively, G_{LNA} refers to the gain of the LNA at the receiver, L_{spread} denotes the loss due to spreading, L_{abs} stands for the absorption loss, L_{mixer} is the conversion loss at receiver and L_{misc} accounts for miscellaneous losses in cables and connectors.

In Fig. 2, the power estimated by utilizing the testbed specifications and the channel model introduced in [27] and the actual received power for a 1.025 THz link are shown. The experimental results closely match the theoretically computed values, which supports our system design and guide us to set the physical layer. Namely, the combination of a very low transmission power (-15 dBm) with the high channel losses leads to very short transmission distances even when utilizing directional antennas (26 dB) simultaneously at the transmitter and the receiver. Challenges in synchronization motivate the use of maximal MF sequences as the frame header.

5.2. Channel frequency characterization

Next, we characterize the THz channel in the vicinity of the first absorption-defined window above 1 THz. The channel frequency characterization is done by generating a constant single tone IF of 500 MHz with the AWG at the transmitter and sweeping the LO frequency at the transmitter and the receiver in fixed steps of 5 GHz, from 1 THz to 1.05 THz. By simultaneously changing the two LOs, we are able to separate the impact of the up & down converters and mixers at the transmitter and the receiver from the actual channel response.

In Fig. 3, we illustrate the measured channel frequency response and compare it to the analytical model first presented in [27]. The numerically predicted and the experimentally measured values at 8 cm and 16 cm are shown. The theoretical channel prediction closely follows the experimentally measured channel response. On the one hand, the results demonstrate the ultra-broadband response of the channel and the THz front-ends, which opens the door to ultra-broadband communication systems. On the other hand, the power fluctuations within the band (up to 5 dB in some cases) emphasize the need for robust channel estimation and equalization schemes, able to operate with multi-GHz bandwidths.

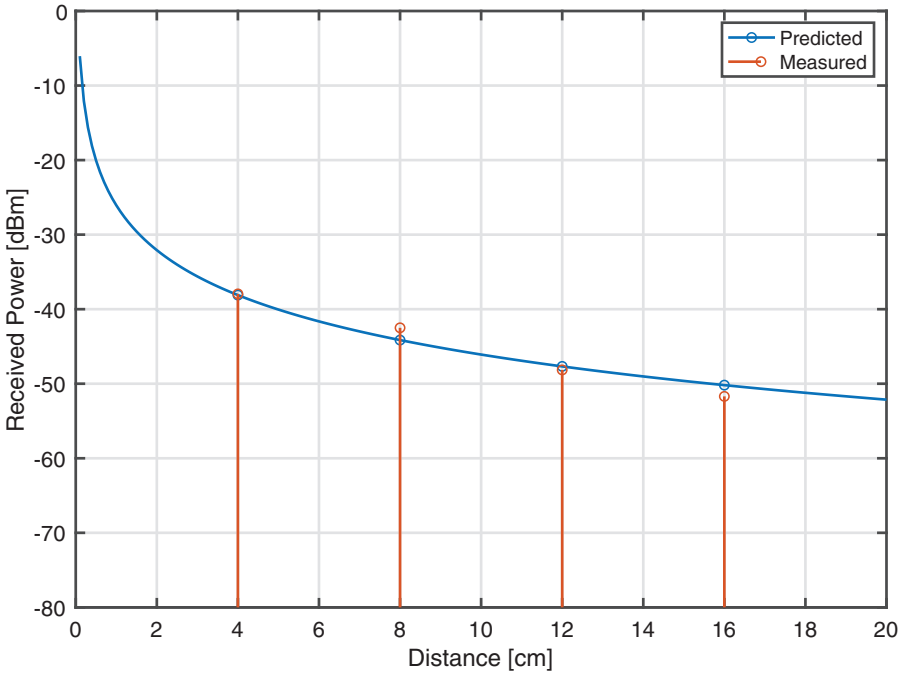

Fig. 2. Comparison between the actual received power and the predicted received power at 1.025 THz as a function of distance.

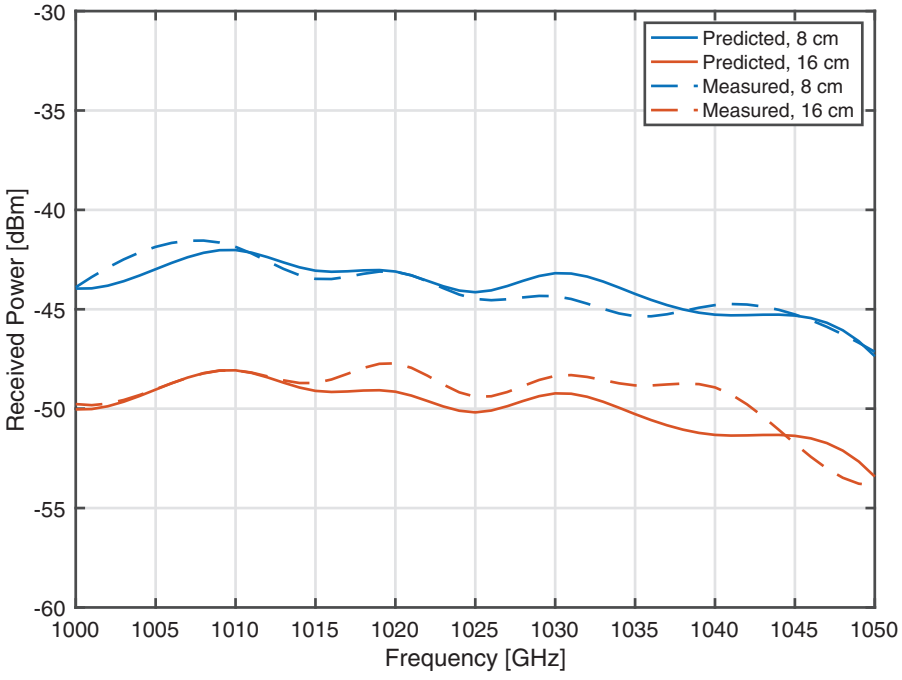

Fig. 3. Comparison between the actual received power and the predicted received power in the 1.0 THz to 1.05 THz range at 8 cm and 16 cm.

5.3. Noise characterization

Noise characterization is an essential step to determine the detection algorithm and required signal processing. The thermal noise in the receiving chain and the absorption noise introduced by water molecules within the channel are the main sources of noise in the TeraNova system. Furthermore, the power supply and the transmission chain introduce low-frequency noise which further impacts the received signals.

The IF noise at the receiver is captured with the DSO. In Fig. 4, the histogram of the measured noise samples is shown. The noise follows a Gaussian distribution, with approximated mean and variance given by -1.7 mV and 2.4 μW, respectively. Therefore, the N_0 value is 3.8×10^{-17} W/Hz for our receiver end. The Gaussian statistics of the noise amplitude justify the implementation of an ML detector at the demodulator.

Another noise type affecting frequency-multiplied systems is phase noise or rapid, short-term, random fluctuations in phase due to time-domain instability of the oscillator. Phase noise is measured against the carrier frequency component, by comparing the carrier power with the power of phase leakage for 1Hz bandwidth at the different phase offset from the carrier frequency. The process gives us the single side band (SSB) phase noise in terms of dBc/Hz (Fig. 4). In the TeraNova platform, the very high stability of the PSG generating the LO results in a very low phase noise at RF of -100 dBc/Hz at 1 MHz, despite the large chain of frequency multipliers. Nevertheless, the phase noise limits the maximum length of the frame. More specifically, given that most of the energy for phase noise is confined within 1 MHz frequency offset, the frame duration should be no longer than 1 μs for the channel estimation and equalization to properly operate. In our system, we select 500 ns as the

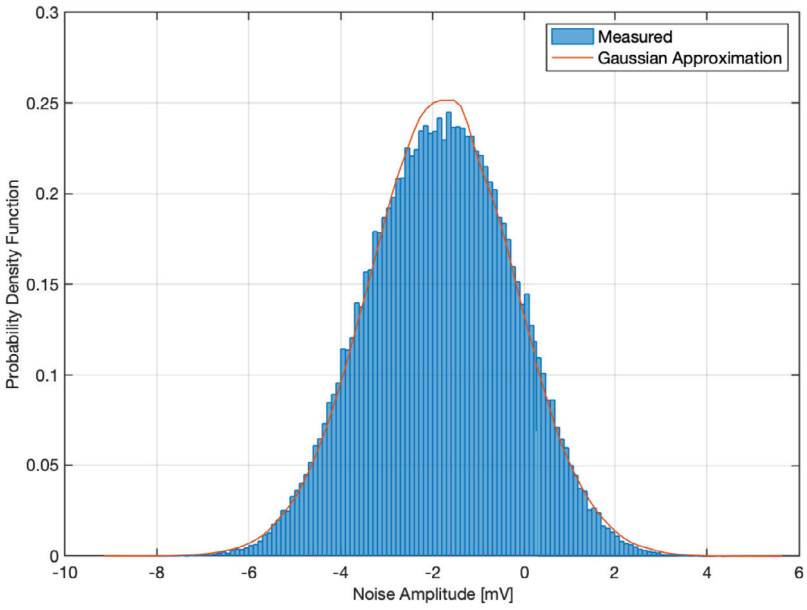

(a) Amplitude noise

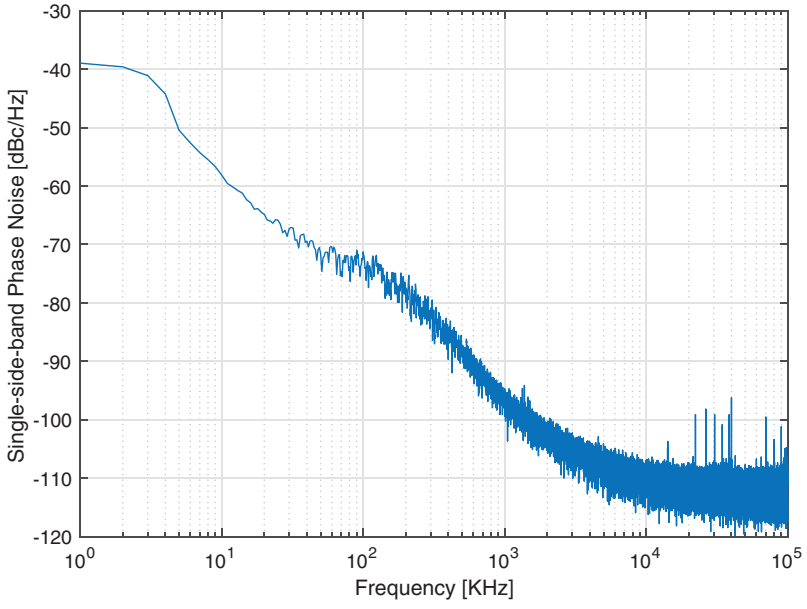

(b) Phase noise

Fig. 4. Noise in the TeraNova testbed: a) PDF of the amplitude noise at the receiver, experimental measurement and numerical approximation; (b) SSB phase noise for the end-to-end system.

approximate maximum duration for our frame, which determines the maximum number of bits per frame presented in Section 4.2.

5.4. Data communication

Based on the experimental hardware and channel characterization, the performance of tailored BPAM, 4PAM, BPSK, QPSK and OFDM modulations at 1 THz, with different modulation bandwidths ranging from 5 GHz to 30 GHz, are experimentally tested. In the case of OFDM, 10 BPSK-modulated subcarriers with 1 GHz bandwidth each are utilized. In Table 2, we summarize our results in terms of number of bit errors for different testbed parameter values, and transmission of fixed-length 2,184 bit packets. Five data frames are considered to estimate the BER. Due to the limitation on the transmitted power, amplitude modulations and, in general, high order modulations, exhibit relatively high BER when the distance increases beyond a few centimeters. In addition, in the case of MPAM, the low-frequency noise is the primary component for the increased bit error. Moreover, the low received power and the frequency-selective response of the end-to-end system combined with the impact of phase noise produce high BER for modulation techniques with a high PAPR, such as OFDM. To mitigate the PAPR by reducing the number of sub carriers, higher sub-carrier bandwidth is utilized for OFDM. In our case, such relatively large bandwidth (1 GHz) does not lessen the ISI performance severely, as the channel is relatively flat within such bandwidth. Moreover, These results motivate the use of phase modulations.

In Fig. 5, the constellation diagram for BPSK and QPSK modulation (16 cm distance with 10 GHz bandwidth) after and before equalization is plotted. Before equalization, the constellations are wide scattered than after equalization, which increases the bit error probability. Therefore, a robust equalization technique is required for THz band communication. It is due to the frequency selective end to end channel and ultra-

Table 2
Measured BER for different modulation schemes.

Modulation	Distance (cm)	BW(GHz) / Bit rate(Gbps)	SNR (dB)	BER
BPSK	6	10 / 5	10	0
BPSK	8	10 / 5	8.5	0
BPSK	12	10 / 5	6	9.1×10^{-5}
BPSK	16	10 / 5	3.5	2.4×10^{-3}
BPSK	6	20 / 10	4	1.8×10^{-4}
BPSK	6	30 / 15	1.8	2.5×10^{-2}
QPSK	6	10 / 10	10	0
QPSK	8	10 / 10	8.5	9.1×10^{-5}
QPSK	12	10 / 10	6	9.1×10^{-4}
QPSK	16	10 / 10	3.5	1.6×10^{-2}
QPSK	6	20 / 20	4	1.2×10^{-3}
QPSK	6	30 / 30	1.8	8.7×10^{-2}
BPAM	6	5 / 5	15.5	0
BPAM	8	5 / 5	14.3	1.8×10^{-4}
BPAM	12	5 / 5	13	5.2×10^{-3}
BPAM	16	5 / 5	8	1.0×10^{-2}
4-PAM	6	5 / 10	12.3	3.7×10^{-2}
4-PAM	8	5 / 10	10	5.1×10^{-2}
OFDM	6	10 / 9	16	7.3×10^{-4}
OFDM	8	10 / 9	13.5	1.0×10^{-2}
OFDM	12	10 / 9	8	5.6×10^{-2}
OFDM	16	10 / 9	3	0.11

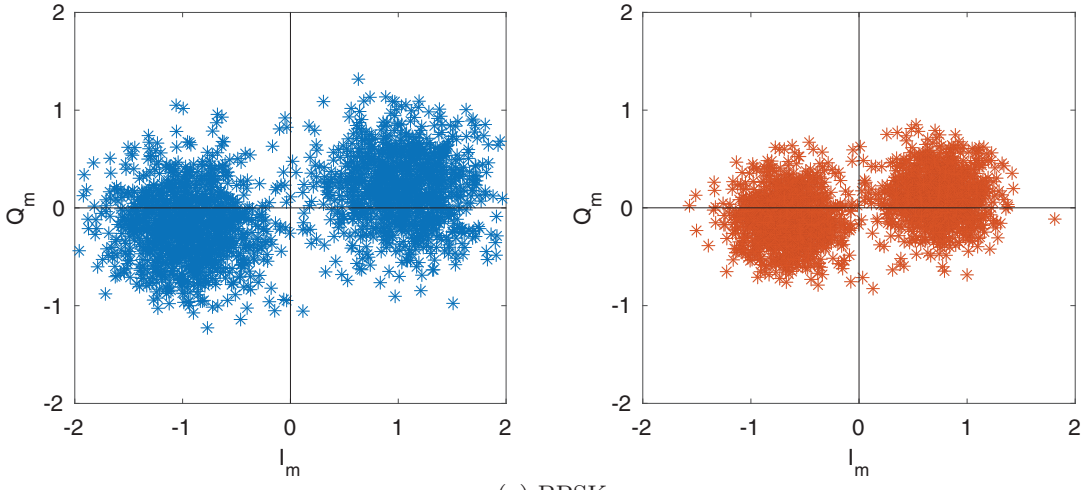

(a) BPSK

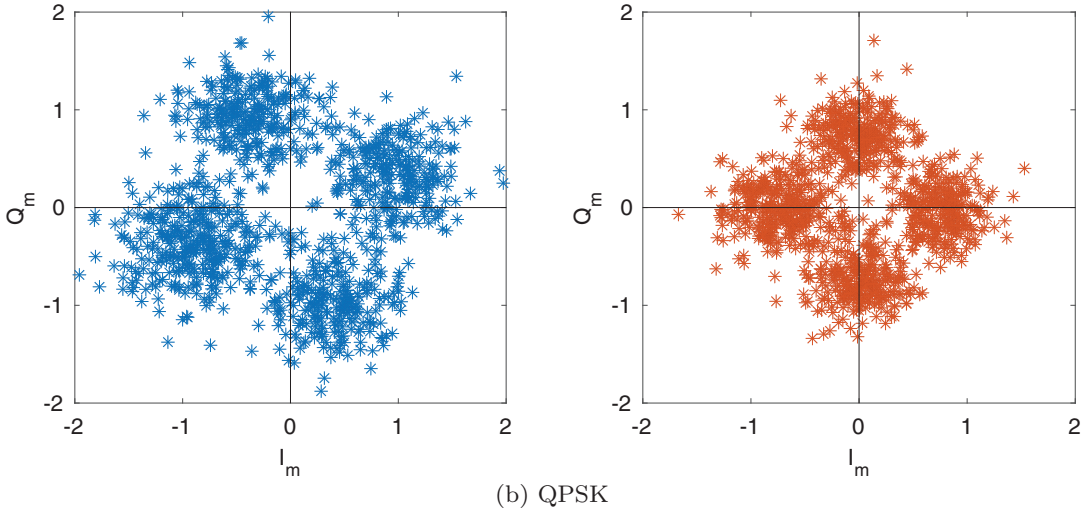

(b) QPSK

Fig. 5. Comparison of the constellation diagram before (left) and after (right) equalization.

broadband nature of the THz band communication. Furthermore, it can help to combat the ISI and multi-path scenario.

6. Next steps

There are several bottlenecks at the physical layer that need to be overcome to unleash the potential of the THz band. The main challenge is posed by the combination of a limited transmission power of THz transmitters with the high path loss of the THz channel. It is relevant to note that, contrary to the popular believe, absorption is not the main problem, even at frequencies above 1 THz. For example, as shown in Fig. 3, at least 50 GHz of consecutive bandwidth is available in our system, and this is in fact limited by the response of the mixers and not of the channel itself. The main contributor to the high path loss is the spreading loss, resulting from the very small effective area of THz antennas. Increasing the effective area intrinsically leads to more directional antennas. While the antennas in the current testbed have *only* 26 dBi gain, lens or dish antennas with higher gains could be utilized. The main challenge in that case is that, due to the very small wavelength of THz signals (e.g., 300 μm at 1 THz), any surface imperfections on the antenna drastically affect its gain. Moreover, while fixed directional antennas can be utilized in static deployments, e.g., backhaul applications, dynamic antenna systems will be needed for mobile applications. Increasing the communication distance thus requires the development of higher-power THz sources, which is an already ongoing task by several groups (for example, the NASA Jet Propulsion Laboratory (JPL) has demonstrated sources with 1 mW at 1 THz [28]) as well as designing (active) antenna arrays able to dynamically beamform, potentially based on new materials and new physics (e.g., graphene plasmonics [29,30]). Currently, no antenna array at 1 THz has been experimentally demonstrated.

Beyond device technology, there are multiple signal processing and communication challenges that need attention. As mentioned before, the very low received signal strength at the receiver makes time and symbol synchronization very challenging. In addition, the highly frequency selective nature of the THz channel requires robust channel estimation and equalization algorithms able to efficiently operate over multi-GHz of consecutive bandwidth in real-time, even within a transmission window and in the case of line-of-sight propagation. For this, techniques inherited from compressed sensing and machine learning (ML) can be utilized. In particular, an ensemble of different artificial Deep Neural Networks (DNN) can be designed and trained to reduce the computational cost associated with critical steps such as channel estimation, channel equalization of the ultra-broadband communication and/or dense antenna arrays [31–33]. Moreover, efficient phase noise estimation and compensation algorithms are needed to mitigate the effect of phase noise introduced by the frequency multiplying chains. Those solutions might be enabled by ML too [34]. The fully software-implemented physical layer in the presented platform enables the rapid testing of new physical layer solutions using this testbed.

All the aspects mentioned above have a direct impact on the received signal power and shape and, ultimately, on the BER. In the current physical layer implementation, we have not incorporated any form of error correction coding technique, because we are interested in understanding the fundamental performance limits. Nevertheless, channel coding can easily be incorporated in software. For the time being, there has been limited research on error correction codes for ultra-broadband THz communications. Among others, low-weight ration codes have been proposed as a way to minimize the impact of multi-user interference and noise at THz frequencies [35], able to outperform conventional Forward Error Correction as well as Automatic Repeat Request strategies [36]. Ultimately, the TeraNova testbed enables the experimental design and testing of new approaches to error control in ultra-broadband networks.

Another major challenge (shared with any high-speed digital communication system) is posed by the sampling rate of DACs and ADCs. With state-of-the-art devices able to support approximately 100 GSaps, the usable bandwidth per carrier is limited to less than 50 GHz. There are two main paths to overcome this bottleneck. On the one hand, multi-band systems, integrated by parallel channels digitally modulated individually and then jointly multiplexed in the analog domain, can be utilized. This, in turn, introduces multiple challenges including carrier synchronization and multiplexing of broadband signals. On the other hand, some of the required functionalities, such as synchronization and channel estimation, can be fully implemented in the analog domain, e.g., by leveraging the state of the art in neuromorphic computing.

Last but not least, we would like to discuss the compactness of the system design. The modular nature of the TeraNova testbed, both in terms of hardware and software, is beneficial for the examination, advancement and expeditious development of the different building blocks of a THz communications link. For example, any frequency multiplier or amplifier in the system can quickly be replaced with a newer design, without the need for a new transceiver. However, this has a direct impact on the system size, as each block needs its own power management and cooling systems. A much compact system could be created by integrating all the blocks (multipliers, amplifiers) in the same chip, but that would require to build an entirely new integrated circuit every time there was an update in an individual block. Similarly, the current system based on Matlab and the AWG/DSO setup ensures a quick transition between fundamental communications and signal processing research and experimental validation. However, the size of the AWG and DSO limit the mobility of the testbed. A custom integrated circuit design implementing a fixed set of communication solutions would result in the most compact platform. As a compromise between the two, the use of a Field Programmable Gate Array (FPGA) solution (e.g., state-of-the-art RF Systems on Chip [37]) could be considered moving forward.

7. Conclusion

In this paper, we have introduced the TeraNova platform, the world's first integrated testbed specific to ultra-broadband communication networks above 1 THz, and reported extensive experimental results to reveal the opportunities and challenges of the THz band. The testbed opens the door to experimental THz research in diverse fields, ranging from the characterization and benchmarking of new THz communication devices to the testing and validation of new channel models and physical layer solutions. Moreover, networking protocols can also be tested by leveraging experimental physical layer traces. Finally, it is our aim to not only utilize, maintain and enhance the current platform, but also to open the platform to the broader wireless communication research community, including from the sharing of the collected data-sets for the results reported in this manuscript in the platform website [38] to facilitating the remote access to the platform to facilitate the test of new building blocks or entirely new software-based solutions.

Declaration of Competing Interest

The authors declare that they have no known competing financial interests or personal relationships that could have appeared to influence the work reported in this paper.

CRediT authorship contribution statement

Priyangshu Sen: Methodology, Software, Writing - original draft. **Dimitris A. Pados:** Conceptualization, Funding acquisition, Methodology, Validation, Writing - review & editing. **Stella N. Batalama:** Conceptualization, Funding acquisition, Validation, Writing - review & editing. **Erik Einarsson:** Conceptualization, Funding acquisition, Validation, Writing - review & editing. **Jonathan P. Bird:** Conceptualization, Funding acquisition, Validation, Writing - review & editing. **Josep M. Jornet:** Conceptualization, Funding acquisition, Methodology, Software, Supervision, Writing - original draft.

Acknowledgement

This work was supported by the U.S. National Science Foundation grants no. CNS-1730148 and CNS-2011411.

Supplementary material

Supplementary material associated with this article can be found, in the online version, at 10.1016/j.comnet.2020.107370.

References

[1] I.F. Akyildiz, J.M. Jornet, C. Han, Terahertz band: next frontier for wireless communications, Phys. Commun. 12 (2014) 16–32.
[2] H. Elayan, O. Amin, B. Shihada, R.M. Shubair, M.S. Alouini, Terahertz band: the last piece of RF spectrum puzzle for communication systems, IEEE Open J. Commun. Soc. 1 (2019) 1–32.
[3] K. Sengupta, T. Nagatsuma, D.M. Mittleman, Terahertz integrated electronic and hybrid electronic–photonic systems, Nat. Electron. 1 (12) (2018) 622–635.
[4] A. Nikpaik, A.H.M. Shirazi, A. Nabavi, S. Mirabbasi, S. Shekhar, A 219-to-231 GHz frequency-multiplier-based VCO with 3% peak DC-to-RF efficiency in 65-nm CMOS, IEEE J. Solid-State Circuits 53 (2) (2018) 389–403.
[5] H. Aghasi, A. Cathelin, E. Afshari, A 0.92-THz sige power radiator based on a nonlinear theory for harmonic generation, IEEE J. Solid-State Circuits 52 (2) (2017) 406–422.
[6] W.R. Deal, T. Foster, M.B. Wong, M. Dion, K. Leong, X.B. Mei, A. Zamora, G. Altvater, K. Kanemori, L. Christen, et al., A 666 GHz demonstration crosslink with 9.5 gbps data rate, in: 2017 IEEE MTT-S International Microwave Symposium (IMS), IEEE, 2017, pp. 233–235.
[7] I. Mehdi, J.V. Siles, C. Lee, E. Schlecht, THz diode technology: status, prospects, and applications, Proc. IEEE 105 (6) (2017) 990–1007.
[8] H.-J. Song, K. Ajito, Y. Muramoto, A. Wakatsuki, T. Nagatsuma, N. Kukutsu, Uni–travelling-carrier photodiode module generating 300 GHz power greater than 1 mw, IEEE Microwave Wirel. Compon. Lett. 22 (7) (2012) 363–365.
[9] S.-W. Huang, J. Yang, S.-H. Yang, M. Yu, D.-L. Kwong, T. Zelevinsky, M. Jarrahi, C.W. Wong, Globally stable microresonator turing pattern formation for coherent high-power THz radiation on-chip, Phys. Rev. X 7 (4) (2017) 41002.
[10] T. Nagatsuma, G. Ducournau, C.C. Renaud, Advances in terahertz communications accelerated by photonics, Nat. Photonics 10 (6) (2016) 371.
[11] Q. Lu, D. Wu, S. Sengupta, S. Slivken, M. Razeghi, Room temperature continuous wave, monolithic tunable THz sources based on highly efficient mid-infrared quantum cascade lasers, Sci. Rep. 6 (2016).
[12] A.C. Ferrari, F. Bonaccorso, V. Fal'Ko, K.S. Novoselov, S. Roche, P. Bøggild, S. Borini, F.H. Koppens, V. Palermo, N. Pugno, et al., Science and technology roadmap for graphene, related two-dimensional crystals, and hybrid systems, Nanoscale 7 (11) (2015) 4598–4810.
[13] C. Jastrow, K. Mu, R. Piesiewicz, T. Ku, M. Koch, T. Kleine-Ostmann, et al., 300GHz transmission system, Electron. Lett. 44 (3) (2008) 213–214.
[14] C. Jastrow, S. Priebe, B. Spitschan, J. Hartmann, M. Jacob, T. Kürner, T. Schrader, T. Kleine-Ostmann, Wireless digital data transmission at 300 GHz, Electron. Lett. 46 (9) (2010) 661–663.
[15] L. Moeller, J. Federici, K. Su, 2.5 gbit/s duobinary signalling with narrow bandwidth 0.625 terahertz source, Electron. Lett. 47 (15) (2011) 856–858.
[16] I. Kallfass, J. Antes, T. Schneider, F. Kurz, D. Lopez-Diaz, S. Diebold, H. Massler, A. Leuther, A. Tessmann, All active MMIC-based wireless communication at 220 GHz, IEEE Trans. Terahertz Sci. Technol. 1 (2) (2011) 477–487.
[17] I. Kallfass, J. Antes, D. Lopez-Diaz, S. Wagner, A. Tessmann, A. Leuther, Broadband active integrated circuits for terahertz communication, in: European Wireless 2012; 18th European Wireless Conference 2012, VDE, 2012, pp. 1–5.
[18] H.-J. Song, K. Ajito, Y. Muramoto, A. Wakatsuki, T. Nagatsuma, N. Kukutsu, 24 gbit/s data transmission in 300 GHz band for future terahertz communications, Electron. Lett. 48 (15) (2012) 953–954.
[19] S. Koenig, D. Lopez-Diaz, J. Antes, F. Boes, R. Henneberger, A. Leuther, A. Tessmann, R. Schmogrow, D. Hillerkuss, R. Palmer, et al., Wireless sub-THz communication system with high data rate, Nat. Photonics 7 (12) (2013) 977.
[20] I. Kallfass, F. Boes, T. Messinger, J. Antes, A. Inam, U. Lewark, A. Tessmann, R. Henneberger, 64 gbit/s transmission over 850 m fixed wireless link at 240 GHz carrier frequency, J. Infrared Millimeter Terahertz Waves 36 (2) (2015) 221–233.
[21] W.R. Deal, T. Foster, M.B. Wong, M. Dion, K. Leong, X.B. Mei, A. Zamora, G. Altvater, K. Kanemori, L. Christen, et al., A 666 GHz demonstration crosslink with 9.5 gbps data rate, in: 2017 IEEE MTT-S International Microwave Symposium (IMS), IEEE, 2017, pp. 233–235.
[22] T. Merkle, A. Tessmann, M. Kuri, S. Wagner, A. Leuther, S. Rey, M. Zink, H.-P. Stulz, M. Riessle, I. Kallfass, et al., Testbed for phased array communications from 275 to 325 GHz, in: 2017 IEEE Compound Semiconductor Integrated Circuit Symposium (CSICS), IEEE, 2017, pp. 1–4.
[23] C. Belem-Goncalves, E. Lacombe, V. Gidel, C. Durand, F. Gianesello, D. Gloria, C. Luxey, G. Ducournau, 300 GHz quadrature phase shift keying and QAM16 56 gbps wireless data links using silicon photonics photodiodes, Electron. Lett. 55 (14) (2019) 808–810.
[24] H. Ganapathy, D.A. Pados, G.N. Karystinos, New bounds and optimal binary signature sets-part II: aperiodic total squared correlation, IEEE Trans. Commun. 59 (5) (2011) 1411–1420.
[25] B.-Y. Chung, C. Chien, H. Samueli, R. Jain, Performance analysis of an all-digital BPSK direct-sequence spread-spectrum IF receiver architecture, IEEE J. Sel. Areas Commun. 11 (7) (1993) 1096–1107.
[26] I. Fujimori, L. Longo, A. Hairapetian, K. Seiyama, S. Kosic, J. Cao, S.L. Chan, A 90-db SNR 2.5-MHz output-rate ADC using cascaded multibit delta-sigma modulation at 8 × oversampling ratio, IEEE J. Solid-State Circuits 35 (12) (2000) 1820–1828.
[27] J.M. Jornet, I.F. Akyildiz, Channel modeling and capacity analysis for electromagnetic wireless nanonetworks in the terahertz band, IEEE Trans. Wireless Commun. 10 (10) (2011) 3211–3221.
[28] J.V. Siles, K.B. Cooper, C. Lee, R.H. Lin, G. Chattopadhyay, I. Mehdi, A new generation of room-temperature frequency-multiplied sources with up to 10 × higher output power in the 160-GHz–1.6-THz range, IEEE Trans. Terahertz Sci. Technol. 8 (6) (2018) 596–604.
[29] A. Singh, M. Andrello, N. Thawdar, J.M. Jornet, Design and operation of a graphene-based plasmonic nano-antenna array for communication in the terahertz band, IEEE JSAC Special Issue on Multiple Antenna Technologies for Beyond 5G, 2020.
[30] I.F. Akyildiz, J.M. Jornet, Realizing ultra-massive MIMO (1024 × 1024) communication in the (0.06–10) terahertz band, Nano Commun. Netw. 8 (2016) 46–54.
[31] D.J. Sebald, J.A. Bucklew, Support vector machine techniques for nonlinear equalization, IEEE Trans. Signal Process. 48 (11) (2000) 3217–3226.
[32] P. Dong, H. Zhang, G.Y. Li, I.S. Gaspar, N. Naderializadeh, Deep CNN-based channel estimation for mmwave massive MIMO systems, IEEE J. Sel. Top. Signal Process. 13 (5) (2019) 989–1000, doi:10.1109/JSTSP.2019.2925975.
[33] E. Giacoumidis, A. Matin, J. Wei, N.J. Doran, L.P. Barry, X. Wang, Blind nonlinearity equalization by machine-learning-based clustering for single-and multichannel coherent optical OFDM, J. Lightwave Technol. 36 (3) (2018) 721–727.
[34] D. Wang, M. Zhang, Z. Cai, Y. Cui, Z. Li, H. Han, M. Fu, B. Luo, Combatting nonlinear phase noise in coherent optical systems with an optimized decision processor based on machine learning, Opt. Commun. 369 (2016) 199–208.
[35] J.M. Jornet, I.F. Akyildiz, Low-weight channel coding for interference mitigation in electromagnetic nanonetworks in the terahertz band, in: 2011 IEEE international conference on communications (ICC), IEEE, 2011, pp. 1–6.
[36] N. Akkari, J.M. Jornet, P. Wang, E. Fadel, L. Elrefaei, G.A. Malik, S. Almasri, I.F. Akyildiz, Joint physical and link layer error control analysis for nanonetworks in the terahertz band, Wirel. Netw. 22 (4) (2016) 1221–1233.
[37] Zynqultrascale + RFSoc systems, https://www.xilinx.com/support/documentation/selection-guides/zynq-usp-rfsoc-product-selection-guide.pdf.
[38] unlab.tech/nano_downloads/teranova/ TeraNova project website.

Priyangshu Sen received the Bachelor of Technology degree from Biju Patnaik University of Technology, India, in 2012. He completed his Industrial training in Garden Reach Shipbuilders and Engineers Limited on the Communication system on naval board ship, in 2011. He started his career as a research engineer at the University of Calcutta in Radio-physics and Electronics in 2013. He received the Master of Technology degree in Radio-physics and Electronics from the University of Calcutta, India, in 2015. He is currently pursuing the Ph.D. degree in the Department of Electrical and Computer Engineering at Northeastern University, Boston, MA, USA, under the guidance of Professor Josep M. Jornet in the UN Lab, MA, USA. In the Summer of 2019, he interned at Samsung Research America. His current research interests are in experimental and statistical characterization of Terahertz communication channel and networks.

Dimitris A. Pados received the Diploma degree in computer science and engineering (five-year program) from the University of Patras, Greece, and the Ph.D. degree in electrical engineering from the University of Virginia, Charlottesville, VA. From 1997 to 2017, he was with the Department of Electrical Engineering, The State University of New York at Buffalo, as Assistant Professor, Associate Professor, Professor, and Clifford C. Furnas Chair Professor of Electrical Engineering. He also served as Associate Chair and was appointed Chair of the Department of Electrical Engineering. He was elected University Faculty Senator four times and served on the Faculty Senate Executive Committee for two terms. In 2017, he joined Florida Atlantic University, Boca Raton, FL, as the Schmidt Chair Professor of Engineering and Computer Science and Fellow of the Institute for Sensing and Embedded Network Systems Engineering (I-SENSE.) Dr. Pados established and directs the FAU Center for Connected Autonomy and Artificial Intelligence. Dr. Pados is a member of the IEEE Communications, IEEE Signal Processing, IEEE Information Theory, and IEEE Computational Intelligence Societies. He served as an Associate Editor for the IEEE Signal Processing Letters and the IEEE Transactions on Neural Networks. For articles that he co-authored with his students received the 2001 IEEE International Conference on Telecommunications Best Paper Award, the 2003 IEEE Transactions on Neural Networks Outstanding Paper Award, the 2010 IEEE International Communications Conference (ICC) Best Paper Award in signal processing for communications, the 2013 International Symposium on Wireless Communication Systems

Best Paper Award in physical layer communications and signal processing, the Best of IEEE GLOBECOM 2014-Top 50 Papers Distinction, and the Best Paper Selection Distinction in the 2016 IEEE International Conference on Multimedia Big Data. He was also the recipient of the 2009 SUNY-wide Chancellor's Award for Excellence in Teaching and the 2011 University at Buffalo Exceptional Scholar-Sustained Achievement Award. Dr. Pados has served as Principal Investigator on federal grants (DoD and NSF) of $12.7M and has been author/coauthor of 220 journal and conference proceedings articles in predominantly IEEE venues. Notable technical contributions from his team include small-sample-support adaptive filtering (auxiliary-vector filters), minimum total-squared-correlation multiple-access code sets (Karystinos-Pados bounds and designs), optimal spread-spectrum data hiding (Gkizeli-Pados-Medley method), L1-norm principal-component analysis (optimal algorithms for exact L1-norm PCA), and robust localization in extreme environments (L1-norm feature extraction from complex-valued data.)

Stella Batalama serves as the Dean of the College of Engineering and Computer Science since August 2017. She served as the Chair of the Electrical Engineering Department, University at Buffalo, The State University of New York, from 2010 to 2017 and as the Associate Dean for Research of the School of Engineering and Applied Sciences from 2009 to 2011. From 2003 to 2004, she was the Acting Director of the AFRL Center for Integrated Transmission and Exploitation, Rome, NY, USA. Her research interests include cognitive and cooperative communications and networks, multimedia security and data hiding, underwater signal processing, communications, and networks. She has published over 180 papers in scientific journals and conference proceedings in her research domain. She was a recipient of the 2015 SUNY Chancellor's Award for Excellence in Research. She was an Associate Editor for the IEEE Communications Letters (2000–2005) and the IEEE Transactions of Communications (2002–2008). Dr. Batalama is a senior member of the Institute of Electrical and Electronics Engineering (IEEE), a member of the Society of Women Engineers, and a member of the American Society for Engineering Education. Dr. Batalama received her Ph.D. in electrical engineering from the University of Virginia and her undergraduate and graduate degrees in computer science and engineering from the University of Patras in Greece. She also completed the Program for Leadership Development at Harvard Business School.

Erik Einarsson received the BS in Physics from the New Mexico Institute of Mining and Technology in 2001, and the MS in Physics from Portland State University in 2003. Erik then moved to Japan, where he completed a Ph.D. in Mechanical Engineering at the University of Tokyo, followed by a two-year postdoctoral fellowship. He then became a Project Assistant Professor at the University of Tokyo until joining the University at Buffalo as an Assistant Professor in 2013, where he currently holds a joint appointment in the Department of Electrical Engineering and the Department of Materials Design and Innovation.

Jonathan Bird joined the faculty of the UB Department of Electrical Engineering as Professor in Fall 2004. More recently, since July 2017, he has been serving in the role of Chair in that Department. He also holds an Adjunct Professor position in the Department of Physics at UB and is a Visiting Professor at Chiba University in Japan. Jonathan obtained his B.Sc. (First-Class Honors) and Ph.D. degrees in Physics from the University of Sussex (United Kingdom), in 1986 and 1990, respectively. He was a JSPS Visiting Fellow at the University of Tsukuba (Japan) from 1991 - 1992, after which he joined the Frontier Research Program of the Institute of Physical and Chemical Research (RIKEN, also in Japan). In 1997, he was appointed as Associate Professor in the Department of Electrical Engineering at Arizona State University, where he spent seven years before joining UB. Prof. Bird's research is in the area of nanoelectronics. He is the co-author of more than 300 peer-reviewed publications, which have been cited more than 7000 times for an h-index of 39, and undergraduate and graduate texts. He is a Fellow of the Institute of Physics and was NYSTAR Distinguished Professor of 2003. His research is currently supported by the Department of Energy, the National Science Foundation and the Air Force Office of Scientific Research.

Josep Miquel Jornet received the B.S. in Telecommunication Engineering and the M.Sc. in Information and Communication Technologies from the Universitat Politécnica de Catalunya, Barcelona, Spain, in 2008. He received the Ph.D. degree in Electrical and Computer Engineering from the Georgia Institute of Technology (Georgia Tech), Atlanta, GA, in 2013. From September 2007 to December 2008, he was a visiting researcher at the Massachusetts Institute of Technology (MIT), Cambridge, under the MIT Sea Grant program. Between August 2013 and August 2019, he was a faculty with the Department of Electrical Engineering at the University at Buffalo, The State University of New York. Since August 2019, he is an Associate Professor in the Department of Electrical and Computer Engineering at Northeastern University in Boston, MA. His current research interests are in Terahertz-band communication networks, Wireless Nano-bio-communication Networks, and the Internet of Nano-Things. In these areas, he has co-authored more than 140 peer-reviewed scientific publications, one book, and has also been granted 3 US patents. Since July 2016, he is the Editor-in-Chief of the Nano Communication Networks (Elsevier) Journal. He is serving as the lead PI on multiple grants from U.S. federal agencies, including the National Science Foundation, the Air Force Office of Scientific Research, and the Air Force Research Laboratory. He is a recipient of the National Science Foundation CAREER award and several other awards from IEEE, ACM, and UB.